Chapter 8
Why Don't We Just Use the Cross Spectra for Operational Modal Analysis?

William Fladung

Abstract The stochastic subspace identification algorithm, which processes correlation functions in the time domain, has been widely used as a specialized parameter estimation method for operational modal analysis for a few decades. It has also been advocated that positive power spectra, which can be derived from response-only cross spectra, can be processed by any frequency-domain parameter estimation algorithm commonly used for experimental modal analysis. This paper proposes that, with some of the currently available algorithms and modern computer speeds, estimating poles directly from cross spectra can be a viable third option.

Keywords operational modal analysis · cross spectra

Introduction

A discussion about modal parameter estimation algorithms employed in the realm of operational modal analysis (OMA) typically begins with an explanation of the frequency response function (FRF) matrix H being the relationship between the responses (or outputs) X and the forces (or inputs) F, which is then multiplied by its conjugate transpose [1, 2].

$$\{X(\omega)\} = [H(\omega)]\{F(\omega)\} \quad \rightarrow \quad \{X(\omega)\}\{X(\omega)\}^H = [H(\omega)]\{F(\omega)\}\{F(\omega)\}^H[H(\omega)]^H \tag{1}$$

With some averaging of the X and F spectra, the XX^H term becomes the output cross-spectra matrix G_{XX}, and the FF^H term becomes the input cross-spectra matrix G_{FF}. Then an assumption is made about the input power spectrum—which is not measured—being "broadband, smooth, and constant," such that it can be excluded from further consideration.

$$[G_{XX}(\omega)] = [H(\omega)][G_{FF}(\omega)][H(\omega)]^H = [H(\omega)][H(\omega)]^H \tag{2}$$

An FRF can be expressed in partial fraction form and in rational fraction polynomial form, and with the denominator polynomial in factored form to show that its roots are the poles $\lambda_r = \sigma_r + j\omega_r$, which occur in conjugate pairs, for $r = 1,\ldots,N$, where N is the number of modes.

$$H(\omega) = \sum_{r=1}^{N} \frac{A_r}{j\omega - \lambda_r} + \frac{A_r^*}{j\omega - \lambda_r^*} = \frac{\sum_{k=0}^{2N-2} (j\omega)^k \beta_k}{\sum_{k=0}^{2N} (j\omega)^k \alpha_k} = \frac{\sum_{k=0}^{2N-2} (j\omega)^k \beta_k}{(j\omega - \lambda_1)(j\omega - \lambda_1^*)\cdots(j\omega - \lambda_N)(j\omega - \lambda_N^*)} \tag{3}$$

The denominators in the partial fraction form of the conjugate of the FRF can also be algebraically coerced into the form of jay-omega-minus-something, where that something just happens to be $-\lambda_r$.

$$H^*(\omega) = \sum_{r=1}^{N} \frac{A_r^*}{(j\omega - \lambda_r)^*} + \frac{(A_r^*)^*}{(j\omega - \lambda_r^*)^*} = \sum_{r=1}^{N} \frac{A_r^*}{-j\omega - \lambda_r^*} + \frac{A_r}{-j\omega - \lambda_r} = \sum_{r=1}^{N} \frac{-A_r}{j\omega - (-\lambda_r)} + \frac{-A_r^*}{j\omega - (-\lambda_r^*)} \tag{4}$$

William Fladung
ATA Engineering, Inc., San Diego, California 92128, USA
e-mail: bill.fladung@ata-e.com

Brandon Dilworth et al. (eds.), *Topics in Modal Analysis & Parameter Identification II, Vol. 10*, Conference Proceedings of the Society for Experimental Mechanics Series, https://doi.org/10.13052/97887-438-0155-9_8

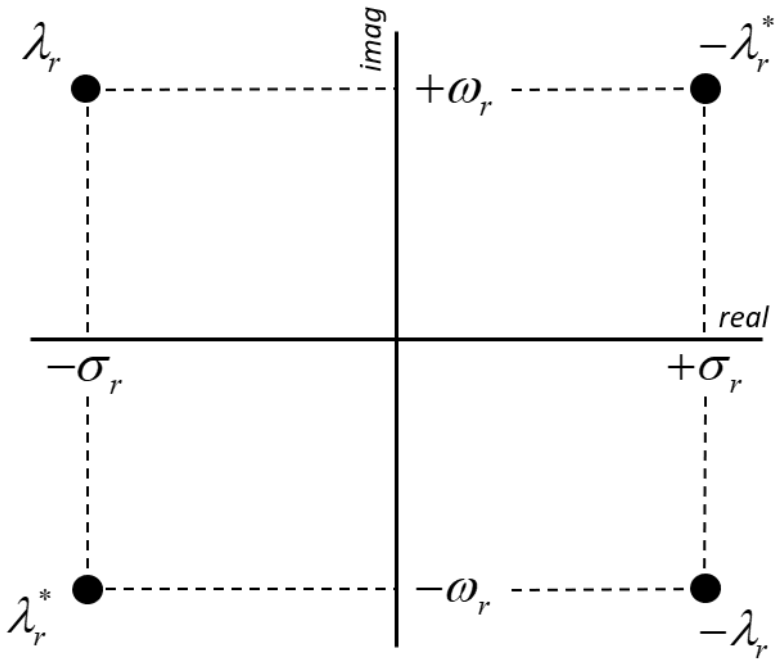

Fig. 1 The quartet of poles contained in a cross spectrum on the complex plane

Whereas an FRF contains pairs of conjugate poles, it can be seen from Eqs. (3) and (4) that a cross spectrum contains quartets of poles, with conjugate pairs of the *positive* poles (λ_r) in the left half plane and conjugate pairs of the *negative* poles ($-\lambda_r$) in the right half plane, as shown in Fig. 1.

Combining H and H^* results in a partial fraction form for a cross spectrum G_{xx} that contains four terms, with two for the positive poles and two for the negative poles. However, the constants in the numerators are no longer true residues A_r because they do not contain modal scaling since the force is not measured.

$$G_{xx}(\omega) = \sum_{r=1}^{N} \frac{R_r}{j\omega - \lambda_r} + \frac{R_r^*}{j\omega - \lambda_r^*} - \frac{\bar{R}_r}{j\omega - (-\lambda_r)} - \frac{\bar{R}_r^*}{j\omega - (-\lambda_r^*)} \tag{5}$$

The inverse Fourier transform of a cross spectrum is a cross correlation, as depicted in Fig. 2a and b. The exponentially decaying response in the positive-lags section of the correlation function corresponds to the positive poles, and the exponentially growing response in the negative-lags section corresponds to the negative poles. A popular OMA method for estimating the poles from the positive-lag section of the correlations is the stochastic subspace identification (SSI) [3] algorithm, but any other time-domain method, such as the polyreference time domain (PTD) [4] algorithm, could also be used.

Alternatively, a *positive power spectrum* (PPS) [1], or *half spectrum* [2], can be created from the Fourier transform of the positive-lags section of the correlation function, as depicted in Fig. 2c and d. Since a PPS contains only the two positive frequency terms in Eq. (5), it has the same partial fraction form as an FRF, and any frequency-domain algorithm can be used to estimate the poles. However, the PPS has a few peculiar traits. The first is that its phase crosses 0° or 180° at resonance (as denoted by the blue markers in Fig. 2d) instead of ±90° as does the phase of an acceleration/force FRF, and all PPSs have this same phase behavior regardless of the response data type. In addition, the act of creating a PPS tends to smooth the function, which often obscures some of the lower peaks, as illustrated in Fig. 3. Truncating a cross correlation to the positive lags (or zeroing the negative lags) has the same effect as multiplying it by a unit step function [1], the Fourier transform of which is $\pi\delta(\omega) + 1/j\omega$ and is shown in the Fig. 3 inset. Convolution of the $1/j\omega$ term with the cross spectrum seems to fill in the valleys between the peaks. This behavior is also evident by comparing Fig. 2a and d.

Furthermore, there is always the possibility of introducing truncation errors when applying the discrete Fourier transform, both when going from the frequency domain to the time domain to produce correlations from cross spectra and again when going back to the frequency domain with the PPS. The former, which would affect time-domain methods such as SSI or PTD, could be avoided by computing correlations in the time domain (which could be time consuming) or by using other signal processing techniques [5]. The latter would be leakage if the correlation response does not decay to zero in the frame of pos-

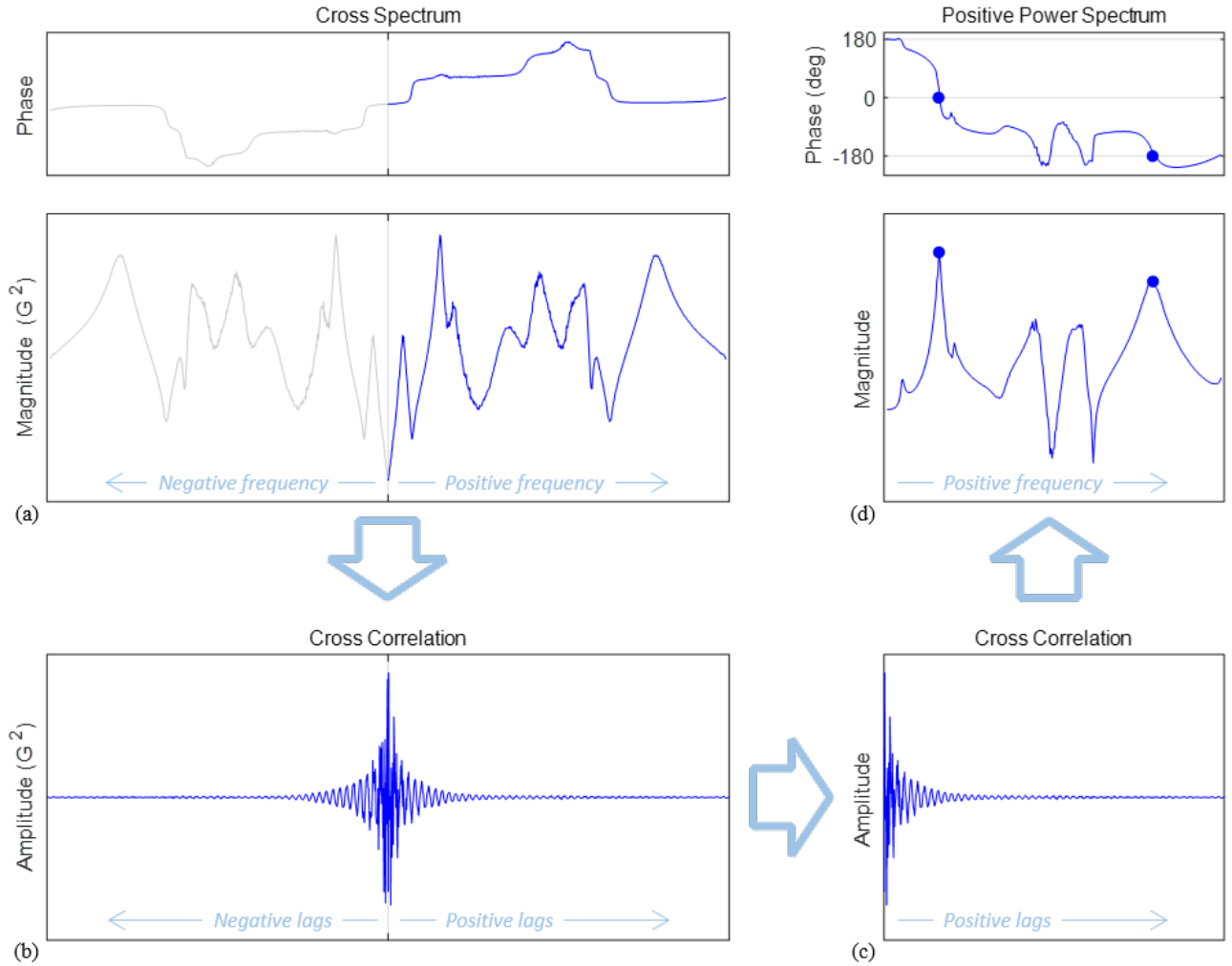

Fig. 2 (a) A double-sided acceleration-to-acceleration cross spectrum, (b) the cross correlation of the cross spectrum in (a), (c) the positive lags of the cross correlation in (b), and (d) the positive power spectrum from the cross-correlation positive lags in (c)

itive lags. Applying an exponential window to the correlations can reduce the effects of leakage [2] but at the expense of artificially increasing the damping, which has the effect of further smoothing the PPS and possibly further obscuring the peaks.

Using Cross Spectra for Estimating Poles

Which brings us to the question posed in the title of this paper. The rational fraction polynomial form of the FRF was given in Eq. (3), and a similar expression for its conjugate is given in Eq. (6), with different (i.e., primed) alpha and beta coefficients and conjugate pairs of the negative poles in the factored form of the denominator polynomial.

$$H^*(\omega) = \frac{\sum_{k=0}^{2N-2} (j\omega)^k \beta'_k}{\sum_{k=0}^{2N} (j\omega)^k \alpha'_k} = \frac{\sum_{k=0}^{2N-2} (j\omega)^k \beta'_k}{(j\omega - (-\lambda_1))(j\omega - (-\lambda_1^*)) \cdots (j\omega - (-\lambda_N))(j\omega - (-\lambda_N^*))} \tag{6}$$

Combining H and H^* to form the cross spectrum as $G_{xx} = HH^*$ produces a rational fraction polynomial model in Eq. (7), with again different (i.e., hatted) alpha and beta coefficients and a characteristic equation in the denominator that has both

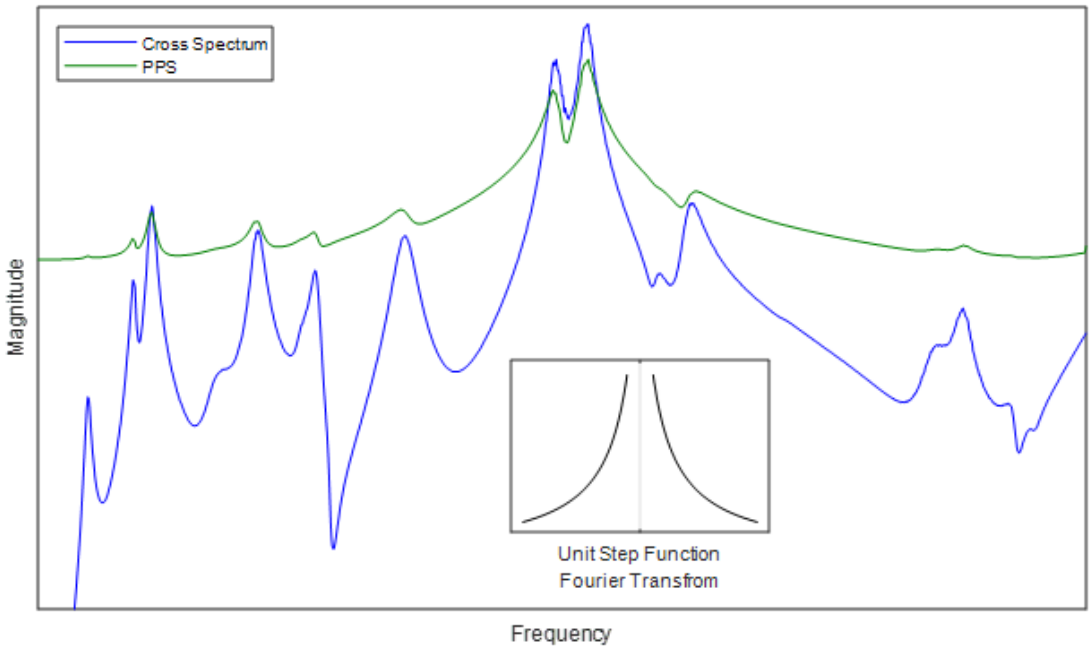

Fig. 3 A cross spectrum and its positive power spectrum

the positive poles (and their conjugates) and the negative poles (and their conjugates) as its roots. The model order of the denominator polynomial is now twice that of an FRF, and the order of the numerator polynomial is 4 less than the order of the denominator polynomial instead of 2.

$$G_{xx} = \frac{\sum_{k=0}^{4N-4} (j\omega)^k \hat{\beta}_k}{(j\omega - \lambda_1)(j\omega - \lambda_1^*) \cdots (j\omega - (-\lambda_1))(j\omega - (-\lambda_1^*)) \cdots (j\omega - (-\lambda_N))(j\omega - (-\lambda_N^*))} = \frac{\sum_{k=0}^{4N-4} (j\omega)^k \hat{\beta}_k}{\sum_{k=0}^{4N} (j\omega)^k \hat{\alpha}_k} \quad (7)$$

Equation (7) forms the basis for extending the rational fraction polynomial (RFP) [6] algorithm to use cross spectra instead of FRFs. A least-squares solution is formulated for the unknown alphas and betas, and an eigenvalue solution of a companion matrix formed with the alphas yields the poles. However, it is well known that the RFP algorithm inevitably becomes ill-conditioned as the frequencies are raised to higher powers, which will only be exacerbated when the model order is doubled. But while this may be true when using high-order models with power polynomials, the ill-conditioning predicament can be evaded by using a different algorithm, such as the Laplace-domain orthogonal polynomial (LDOP) [7] algorithm or the Z-domain orthogonal polynomial (ZDOP) [8] algorithm. These two algorithms are similar to their ancestor RFP in that they are high-order models with the alpha coefficients being the size of the number of references—but instead of power polynomials, their basis functions are orthogonal polynomials (in either the Laplace or Z domain), which have favorable numerical conditioning characteristics regardless of the model order. In addition, the polyreference least-squares complex frequency (PLSCF) [9] and the z-domain rational fraction polynomial (RFP-Z) [10] algorithms use a complex frequency mapping to the z-domain to forgo the use of power polynomials, making them viable candidates for using cross spectra for OMA as well. A low-order frequency-domain algorithm [10], which has coefficient matrices the size of the number of responses and a model order of 2, could also be adapted for OMA with cross spectra by using a model order of 4.

For a modal test (i.e., the kind where the excitation is supplied by shakers and the forces are measured), the number of references is typically less than about ten and much less than the number of responses, which could be as many as a few hundred. For an OMA test, there could also be hundreds of response channels measured. The $N_o \times N_o$ output cross-spectra matrix $[G_{XX}]$ in Eq. (2) is created (at each frequency) by the outer product of the $N_o \times 1$ vector of responses $\{X\}$ from Eq. (1), which means that there would be N_o references, too. Obviously, using hundreds of references in a high-order algorithm such as RFP, ZDOP, LDOP, PLSCF, or RFP-Z would generate an impractically large number of poles as the model order increases. While the response channels could be down-selected to a more reasonable number of references, the criteria

Table 1 Time trials of ZDOP solutions using PPS and cross spectra

Spectral Lines	Responses	References	Minimum Order	Step Order	Maximum Order	PPS	Cross Spectra
1600	100	5	10	2	40	3 s	9 s
1600	100	10	5	1	20	3 s	10 s
1600	200	5	10	2	40	5 s	15 s
1600	200	10	5	1	20	5 s	17 s

for doing so may not be overly intuitive. Alternatively, the reference space could be condensed to a few *virtual references* using a subset of vectors from the singular value decomposition of a concatenated array of G_{XX} at all spectral lines over the frequency range of interest.

Some preemptive time trials were run for a few feasibly large datasets, with the results listed in Table 1. The number of poles produced from the characteristic equation is equal to the model order times the size of the coefficient matrices, which for a high-order model such as ZDOP is the number of references. The model orders listed in Table 1 correspond $2N$ in the denominator polynomials in Eqs. (3) and (6), and the model orders for the cross spectra were double those listed. The number of spectral lines corresponds to the originating cross spectra and the PPS have half that many (and double the frequency spacing) after the negative lags are truncated. Unsurprisingly, solving for twice the model order takes longer to complete—three or more times longer from a relative point of view. But in actual time that somebody would have to wait, it's only a few more seconds.

As a proof of concept, poles were estimated from a random excitation test run on an "iron bird" laboratory test article, shown in Fig. 4a. There was a vertical shaker attached to both of the wings and horizontal stabilizers, as indicated by the arrows, and 109 responses. Cross spectra were generated from the FRFs as HH^H, and PPSs were generated from the cross spectra. Although this is admittedly not an OMA test, $[G_{FF}]$ in Eq. (2) is truly an identity matrix in this case, and the stability diagram for the FRFs in Fig. 4b serves as the baseline for evaluating the PPS and cross-spectra results. The gold stars in the top row are autonomously selected poles [11–13], and the filled blue squares are manually selected poles. The stability diagram for PPSs is shown in Fig. 5a, and the stability diagram for cross spectra is shown in Fig. 5b. The model orders on the y-axis of the stability diagrams correspond to the positive poles of the underlying FRF model (i.e., $2N$ in the denominator polynomials in Eqs. (3) and (6)), and the model orders for the cross-spectra solutions were double those. Using the ZDOP algorithm with zero$^{\text{th}}$-order coefficient normalization yields clear stability diagrams [14] for all three, with quite

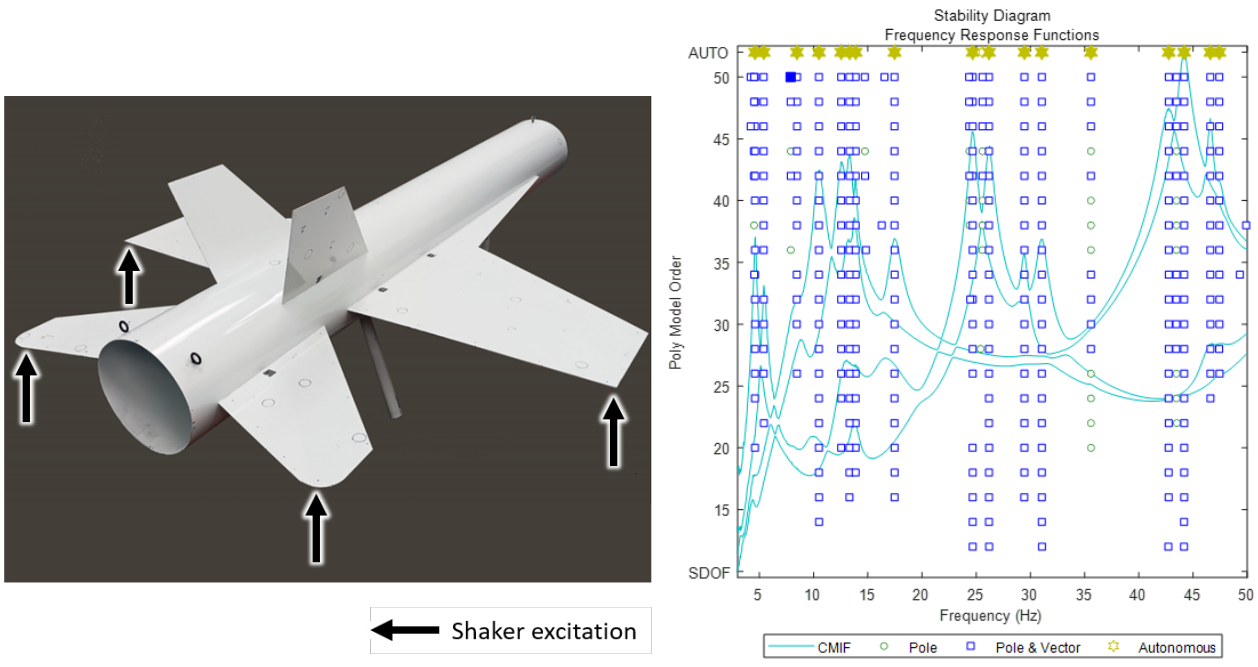

(a) (b)

Fig. 4 (a) The iron bird laboratory test article; (b) ZDOP stability diagram for FRFs

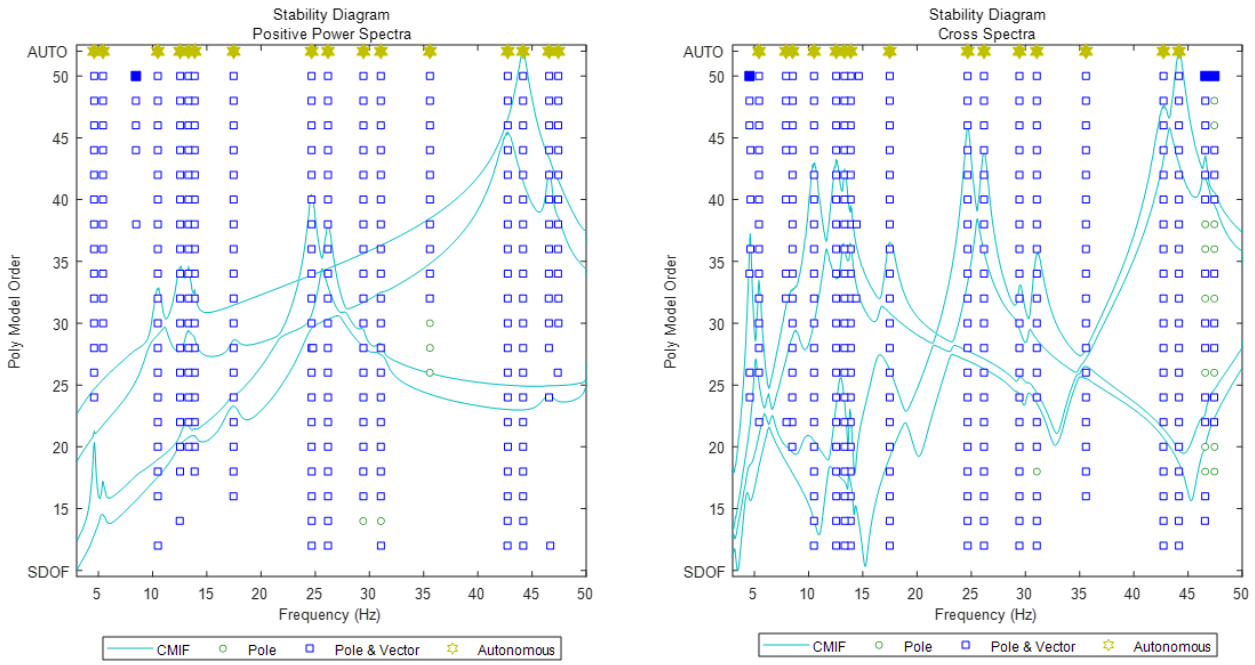

Fig. 5 (a) ZDOP stability diagram for PPS; (b) ZDOP stability diagram for cross spectra

satisfactory and generally comparable results. One exception is that while a few consistent poles at 8.5 Hz were found with PPS for higher model orders, the mode at 7.9 Hz was missed entirely, and there's no evidence of either in the mode indicator functions. The frequency and damping values for the selected poles from the three stability diagrams are listed in Table 2, which verifies that the frequencies match well, albeit with some disagreement about the damping for a few of the modes.

Table 2 Selected poles from stability diagrams in Fig. 4b and Fig. 5

	FRF		PPS		Cross Spectra	
Mode No.	**Frequency (Hz)**	**Damping (%)**	**Frequency (Hz)**	**Damping (%)**	**Frequency (Hz)**	**Damping (%)**
1	4.59	2.04	4.60	2.19	4.55	3.02
2	5.39	3.37	5.42	3.53	5.42	4.33
3	7.88	8.51	—	—	7.92	7.38
4	8.46	7.90	8.46	7.96	8.52	8.06
5	10.49	3.55	10.48	3.59	10.50	3.58
6	12.54	3.03	12.54	2.92	12.55	2.99
7	13.32	1.75	13.31	1.62	13.31	1.62
8	13.88	0.92	13.88	0.90	13.88	0.92
9	17.46	3.04	17.47	3.02	17.48	3.04
10	24.67	1.18	24.67	1.17	24.67	1.12
11	26.18	1.29	26.17	1.27	26.18	1.25
12	29.45	1.03	29.45	1.02	29.45	1.03
13	31.05	1.53	31.05	1.53	31.05	1.53
14	35.58	1.30	35.58	1.30	35.58	1.30
15	42.76	1.63	42.76	1.58	42.73	1.62
16	44.18	0.98	44.17	0.96	44.16	0.95
17	46.60	0.53	46.58	0.52	46.59	0.50
18	47.42	0.99	47.42	0.76	47.43	0.85

Using Cross Spectra for Estimating Residues

It should come as no surprise that the partial fraction model for residue estimation has four terms for each mode. Modifying Eq. (5) by collecting the terms in the summation and including residuals gives the single-reference residues estimation formulation as

$$G_{xx}(\omega) = \sum_{r=1}^{4N} \frac{R'}{j\omega - \lambda_r} + \left(\frac{1}{\omega^2}\right)^2 \rho_L + (1)^2 \rho_U, \tag{8}$$

where $4N$ in the upper limit of the summation signifies quartets of poles, *R'* (i.e., prime) stands in for both variants of the *R*'s and their conjugates in Eq. (5), λ_r can be either a positive or negative pole, ρ_L is the lower residuals, and ρ_U is the upper residuals. The residual terms, which are derived from the asymptotic behavior of a single degree of freedom FRF far away from its resonance, need to be squared since the cross spectrum is defined from HH^H. A least-squares solution for the residues and residuals is generated by rearranging Eq. (8) into matrix form and evaluating at different frequencies.

$$\begin{bmatrix} G_{xx}(\omega_1) \\ G_{xx}(\omega_2) \\ G_{xx}(\omega_3) \\ \vdots \end{bmatrix} = \left[\begin{array}{ccc|cc} \Lambda_1(\omega_1) & \cdots & \Lambda_{4N}(\omega_1) & \omega_1^{-4} & 1 \\ \Lambda_1(\omega_2) & \cdots & \Lambda_{4N}(\omega_2) & \omega_2^{-4} & 1 \\ \Lambda_1(\omega_3) & \cdots & \Lambda_{4N}(\omega_3) & \omega_3^{-4} & 1 \\ \vdots & & \vdots & \vdots & \vdots \end{array}\right] \left[\begin{array}{c} R'_1 \\ \vdots \\ R'_{4N} \\ \hline \rho_L \\ \rho_U \end{array}\right], \quad \text{where } \Lambda_r(\omega) = \frac{1}{j\omega - \lambda_r} \tag{9}$$

In general, the residues are (or can be) complex, but a phase-constrained least-squares solution for real (or normal) mode shapes [15] can be formulated by partitioning the *Ax* = *b* form of Eq. (9) as

$$\hat{A}\hat{x} + c_L\rho_L + c_U\rho_U = b, \quad \text{where } \hat{x} = \begin{bmatrix} R'_1 & \cdots & R'_{4N} \end{bmatrix}^T, c_L = \omega^{-4}, c_U = 1, \tag{10}$$

$\hat{A}$ is the left partition of *A*, *b* is the cross spectrum, and ρ_L and ρ_U are real such that the residual terms are purely real. Then expand the complex terms into their real and imaginary parts as

$$\left(\hat{A}_r + j\hat{A}_i\right)(\hat{x}_r + j\hat{x}_i) + c_L\rho_L + c_U\rho_U = b_r + jb_i, \quad \text{where } \hat{A}_r = \text{Re}\left(\hat{A}\right), \hat{A}_i = \text{Im}\left(\hat{A}\right), \tag{11}$$

and likewise for $\hat{x}$ and *b*. Next, expand the product of the two complex terms and collect the real and imaginary components into separate equations as

$$\begin{aligned} \hat{A}_r\hat{x}_r - \hat{A}_i\hat{x}_i + c_L\rho_L + c_U\rho_U &= b_r \\ \hat{A}_i\hat{x}_r + \hat{A}_r\hat{x}_i &= b_i \end{aligned} \tag{12}$$

The response and reference (i.e., force) of an FRF are 90° out of phase at resonance and the residue is purely imaginary, which means $\hat{x}_r = 0$ for real mode shapes. However, response and reference of a cross spectrum are really both responses (e.g., acceleration) and must be either in phase (i.e., 0°) or out of phase (i.e., 180°) for a real mode shape, which means that the residue must be purely real and $\hat{x}_i = 0$. Removing those terms and combining into matrix form gives the normal mode solution as

$$\begin{bmatrix} \hat{A}_r & c_L & c_U \\ \hat{A}_i & 0 & 0 \end{bmatrix} \begin{Bmatrix} \hat{x}_r \\ \rho_L \\ \rho_U \end{Bmatrix} = \begin{Bmatrix} b_r \\ b_i \end{Bmatrix} \tag{13}$$

The above alterations to the residues algorithm (i.e., four terms in the summation, squaring of the residuals, and real shape coefficients) are also applicable to the multiple-reference formulation.

Figure 6 shows the complex mode indicator function (CMIF) computed from the measured cross spectra (b) and from the PPS derived from the measured cross spectra (a). Also plotted are the CMIFs computed from the cross spectra and PPS synthesized with the poles in Table 2 and estimated residues. For both cases, the synthesized functions match well with the measured functions at the prominent peaks but not as well at the less well excited (and less well indicated) peaks. The modal assurance criteria (MAC) between shapes from the FRFs and from the PPS and cross spectra, shown in Fig. 7, reach the same consensus, with the shapes matching well for well excited (and well indicated) modes but less so otherwise.

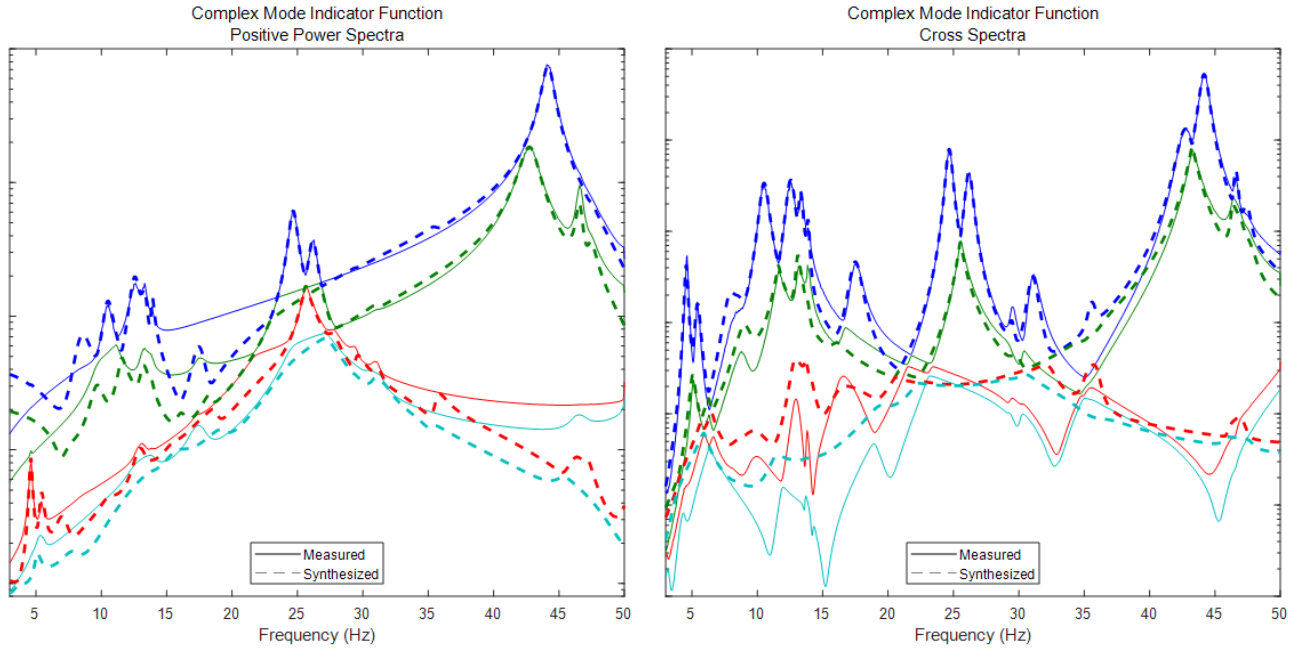

(a) (b)

Fig. 6 (a) CMIF from measured and synthesized PPS; (b) CMIF from measured and synthesized cross spectra

Cross MAC Table
FRF Shapes

PPS Shapes		1 4.59	2 5.40	3 7.91	4 8.49	5 10.49	6 12.55	7 13.32	8 13.88	9 17.47	10 24.67	11 26.18	12 29.45	13 31.05	14 35.58	15 42.76	16 44.18	17 46.60	18 47.43
1	4.61	86									29								
2	5.43		59								28	29							
3	8.49																96		
4	10.49					95										36			
5	12.54				29		85										45		
6	13.31							90											
7	13.88							24									73		
8	17.48					23				34						69			
9	24.67										100								
10	26.17											100							
11	29.45																75		
12	31.05					25								62		44			
13	35.58																95		
14	42.76															99			
15	44.17																100		
16	46.58																	91	27
17	47.42															25		36	

(a)

Cross MAC Table
FRF Shapes

XSPEC Shapes		1 4.56	2 5.42	3 7.94	4 8.55	5 10.51	6 12.55	7 13.31	8 13.88	9 17.49	10 24.67	11 26.18	12 29.45	13 31.05	14 35.58	15 42.74	16 44.16	17 46.59	18 47.44
1	4.56	98																	
2	5.42		72																
3	7.94															40			
4	8.55				51												34		
5	10.51					99													
6	12.55				27		97												
7	13.31							98											
8	13.88							78	32										
9	17.49					24				85									
10	24.67										100								
11	26.18											100							
12	29.45											54							
13	31.05													88					
14	35.58															47	44		
15	42.74															99			
16	44.16																100		
17	46.59																	96	31
18	47.44																	44	

(b)

Fig. 7 (a) Cross-MAC for FRF shapes vs PPS shapes; (b) cross-MAC for FRF shapes vs cross-spectra shapes

Missing Phase Crossings at Resonance

Figure 8a shows two FRFs from the wingtips of another mock aircraft test article (shown in the inset). The drive point FRF exhibits the expected phase characteristics with drops through 90° at resonance (indicated by the black markers). The FRF for the opposite wingtip also has phase drops through ±90° at resonance, with the first and fourth modes in phase and second and third modes out of phase. Figure 8b shows the cross spectra for the responses of the FRFs in Fig. 8a, generated from HH^H. The cross spectrum for the drive point response, which is actually an auto spectrum, has phase of zero at all frequencies. The phase of the cross spectrum for the opposite wingtip is again in phase (i.e., −360°) for the first and fourth modes and out of phase (i.e., −180°) for the second and third modes. Thus, one compromise inherent to using cross spectra for OMA is the missing phase crossings at resonance, which can sometimes offer another opinion when evaluating the estimated poles. For example, the phase crossing can verify the undamped natural frequency and the slope of the phase can assess the damping of a heavily damped mode that may not have a distinct peak indicating the resonance.

As a side effect of cross spectra not having ±90° phase crossings at resonance, the normal mode indicator function (NMIF) and the multivariate mode indicator function (MMIF) cannot be used with cross spectra. This is because the NMIF is derived from the ratio of the real part to the magnitude of FRFs, and the drops in the functions occur when the real part is

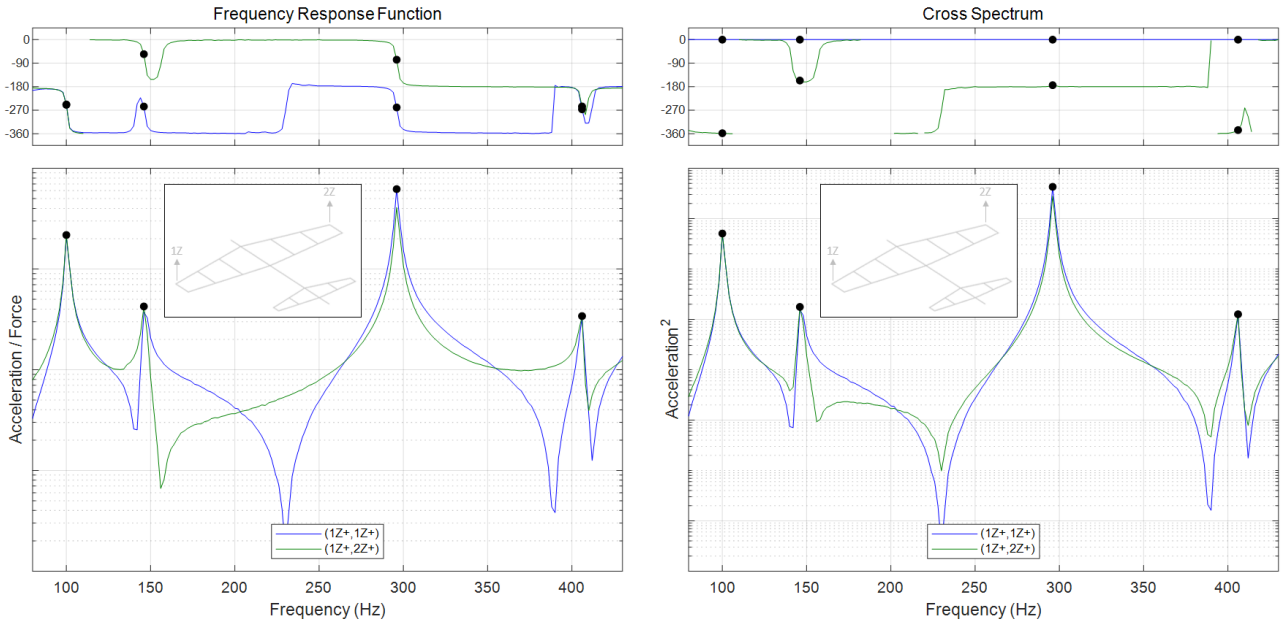

Fig. 8 (a) Two mock airplane wingtip FRFs; (b) cross spectra for responses of the FRFs in (a)

zero, which is the same as a phase of 90°. The same reason applies to the MMIF, since it is the multiple-reference extension of the NMIF [16].

Summary

Whereas correlation functions and PPS have conventionally been used for OMA parameter estimation, this paper has shown that, with a prudent choice of an algorithm and a bit of patience, so too can cross spectra. A quartet of positive and negative poles is estimated from cross spectra, requiring twice the model order and more than twice the time. But while the computational burden might have been an obstacle in the past, today the additional wait time should only be a few seconds. The residue estimation formulation is also adaptable to cross spectra for either complex or real shapes. The benefits of using cross spectra are being able to use standard spectral estimation methods and avoiding any potentially error-inducing trips between the temporal domains. Of course, there are necessarily trade-offs with using cross spectra, such as not having $\pm 90°$ phase crossings at resonance and not being able use certain mode indicator functions.

References

1. Chauhan, S., Martell, R., Allemang, R.J., and Brown. D.L., "Unified Matrix Polynomial Approach for Operational Modal Analysis," *Proceedings of the 25th International Modal Analysis Conference*, February 2007.
2. Peeters, B., and Van der Auweraer, H., "PolyMax: a revolution in operational modal analysis," *Proceedings of the 1st International Operational Modal Analysis Conference*, April 2005.
3. Chauhan, S., "Using the Unified Matrix Polynomial Approach (UMPA) for the Development of the Stochastic Subspace Identification (SSI) Algorithm," *Journal of Vibration and Control*, Vol. 19, No. 13, pp. 1950–61, October 2013.
4. Vold, H., Kundrat, J., Rocklin, T., and Russell, R., "A Multi-Input Modal Estimation Algorithm for Mini-Computers," *SAE Transactions*, Vol. 91, No. 1, pp. 815–21, January 1982.
5. Xu, Y.F., Liu, J.M., and Zhu, W.D., "Accurate and Efficient Calculation of Discrete Correlation Functions and Power Spectra," *Journal of Sound and Vibration*, Vol. 347, pp. 246–65, July 2015.
6. Richardson, M., and Formenti, D.L., "Parameter Estimation from Frequency Response Measurements Using Rational Fraction Polynomials," *Proceedings of the 1st International Modal Analysis Conference*, 1982.

7. Fladung, W.,and H. Vold, “An Orthogonal View of the Polyreference Least-Squares Complex Frequency Modal Parameter Estimation Algorithm,” *Proceedings of the 33rd International Modal Analysis Conference*, February 2015.
8. Fladung, W., and H. Vold, “An Improved Implementation of the Orthogonal Polynomial Modal Parameter Estimation Algorithm Using the Orthogonal Complement,” *Proceedings of the 33rd International Modal Analysis Conference*, February 2015.
9. Guillaume, P., Verboven, P., Vanlanduit, S., Van der Auweraer, H., and Peeters, B., “A Poly-Reference Implementation of the Least-Squares Complex Frequency-Domain Estimator,” *Proceedings of the 21st International Modal Analysis Conference*, February 2003.
10. Chauhan, S., Martell, R., Allemang, R.J., and Brown. D.L., “Implementation of Complex Frequency Mapping to Low Order Frequency Domain algorithm for Operational Modal Analysis,” *Proceedings of the 25th International Modal Analysis Conference*, February 2007.
11. Phillips, A.W., Allemang, R.J., and Brown, D.L., “Autonomous Modal Parameter Estimation: Methodology,” *Proceedings of the 29th International Modal Analysis Conference*, February 2011.
12. Phillips, A.W., Allemang, R.J., and Brown, D.L., “Autonomous Modal Parameter Estimation: Statistical Considerations,” *Proceedings of the 29th International Modal Analysis Conference*, February 2011.
13. Phillips, A.W., Allemang, R.J., and Brown, D.L., “Autonomous Modal Parameter Estimation: Application Examples,” *Proceedings of the 29th International Modal Analysis Conference*, February 2011.
14. Verboven, P., Cauberghe, B., Vanlanduit, S., Parloo, E., and Guillaume, P., “The Secret Behind Clear Stabilization Diagrams: The Influence of the Parameter Constraint on the Stability of the Poles,” *Proceedings, Society of Experimental Mechanics (SEM) Annual Conference*, 2004.
15. Fladung, W., and Napolitano, K., “Tips, Tricks, and Obscure Features for Modal Parameter Estimation,” *Proceedings of the 41st International Modal Analysis Conference*, February 2023.
16. Williams, R., Crowley, J., Vold, H., “The Multivariate Mode Indicator Function in Modal Analysis,” *Proceedings of the 3rd International* Modal Analysis Conference, 1985.